
Exact Information Bottleneck with Invertible Neural Networks: Getting the Best of Discriminative and Generative Modeling

Lynton Ardizzone^{*1}, Radek Mackowiak^{*2}, Ullrich Kthe¹, Carsten Rother¹

¹ Visual Learning Lab, Heidelberg University, Heidelberg, Germany,

² Robert Bosch Corporate Research - Computer Vision, Hildesheim, Germany

* These authors contributed equally to this work

Abstract

The Information Bottleneck (IB) principle offers a unified approach to many learning and prediction problems. Although optimal in an information-theoretic sense, practical applications of IB are hampered by a lack of accurate high-dimensional estimators of mutual information, its main constituent. We propose to combine IB with invertible neural networks (INNs), which for the first time allows exact calculation of the required mutual information. Applied to classification, our proposed method results in a generative classifier we call IB-INN. It accurately models the class conditional likelihoods, generalizes well to unseen data and reliably recognizes out-of-distribution examples. In contrast to existing generative classifiers, these advantages incur only minor reductions in classification accuracy in comparison to corresponding discriminative methods such as feed-forward networks. Furthermore, we provide insight into why IB-INNs are superior to other generative architectures and training procedures and show experimentally that our method outperforms alternative models of comparable complexity.

Code available at github.com/VLL-HD/FrEIA

1 INTRODUCTION

The distinction between discriminative and generative classifiers (DCs vs. GCs) is fundamental to machine learning. DCs directly predict posterior class probabilities $p(Y|X)$, where X and Y denote input and output variables respectively. GCs instead model the joint probability $p(X, Y)$, usually as a product of class priors $p(Y)$ and conditional data likelihoods $p(X|Y)$. They are able to generate synthetic data, and poste-

rior class probabilities can simply be inferred by Bayes' rule $p(Y|X) = p(X|Y)p(Y)/\mathbb{E}_{p(Y)} [p(X|Y)]$.

DCs optimize prediction performance directly and therefore achieve better results in this respect. However, their models for $p(Y|X)$ tend to be most accurate near decision boundaries (where it matters), but deteriorate away from them (where deviations incur no noticeable loss). Consequently, they are poorly calibrated (Guo et al., 2017) and out-of-distribution data can not be recognized at test time (Ovadia et al., 2019). In contrast, GCs model full likelihoods $p(X|Y)$ and thus implicitly full posteriors $p(Y|X)$, which leads to the opposite behavior – better predictive uncertainty at the price of reduced accuracy. In-depth studies of the involved trade-offs (Bishop & Lasserre, 2007; Bishop, 2007) revealed a hyperparameter, which controls the balance between discriminative and generative performance. However, models trained with traditional loss functions (in particular maximum likelihood) typically exhibit unsatisfactory accuracy even at optimal hyperparameter settings, so that recent work has called into question the overall effectiveness of GCs (Fetaya et al., 2019; Nalisnick et al., 2019). We argue in the following that these works may be overly pessimistic, as they do not consider alternative training methods.

As an alternative, we apply the Information Bottleneck (IB) objective (Tishby et al., 2000) to generative classification. IB formulates the discriminative/generative trade-off in a very general information-theoretic form. It postulates existence of a latent space Z , where all information flow between X and Y is channeled through (hence the method's name). In order to optimize predictive performance, IB attempts to maximize the mutual information $I(Y, Z)$ between Y and Z . Jointly, it strives to minimize the mutual information $I(X, Z)$ between X and Z , forcing the model to ignore irrelevant aspects of X , which do not contribute to classification performance and only increase the potential for overfitting.

Unfortunately, practical application of IB as a loss

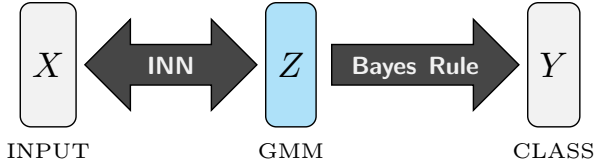


Figure 1: Our generative classifier as the Information Bottleneck Invertible Neural Network (IB-INN).

function is difficult because existing estimators for mutual information (MI) are not sufficiently reliable in high dimensions. The Variational Information Bottleneck (VIB, Alemi et al., 2017; Kolchinsky et al., 2017) provides a feasible approximation in form of an upper bound for IB, which however does not work as well as the asymptotically exact solution presented in this work.

Using Invertible Neural Networks (INNs), we can, for the first time, train generative classifiers directly with the IB objective, cf. Fig. 1. This major advance arises from two critical properties of this network type: (i) the transformation between X and Z has a tractable Jacobian determinant, and (ii) the latent space Z can be shaped as a Gaussian Mixture Model (GMM). As a result, the IB objective is analytically expressible in terms of the change-of-variables formula, allowing for standard gradient descent training without additional approximations. Moreover, properties (i) and (ii) facilitate latent space exploration and thus enable out-of-distribution detection and the analysis of class similarities. The Lagrange multiplier β occurring in the IB loss (4) allows us to explicitly alter the trade-off between our model’s classification performance and its generative modeling capabilities. When β is adjusted properly, our experiments reveal that IB-INNs simultaneously exhibit high predictive accuracy, well calibrated uncertainties and allow to reliably detect out-of-distribution examples.

To summarize, we combine two concepts – the Information Bottleneck (IB) objective and Invertible Neural Networks (INNs) – into a new generative classifier type called IB-INN. Our contributions are as follows:

- We derive an asymptotically exact formulation of the IB loss for a special GC type by utilizing INNs.
- We show experimentally that our models outperform existing GCs on CIFAR10/CIFAR100 in terms of classification error, and incur at worst minor degradation relative to feed-forward DCs.
- We demonstrate good uncertainty quantification in terms of accurate posterior calibration and reliable outlier detection.

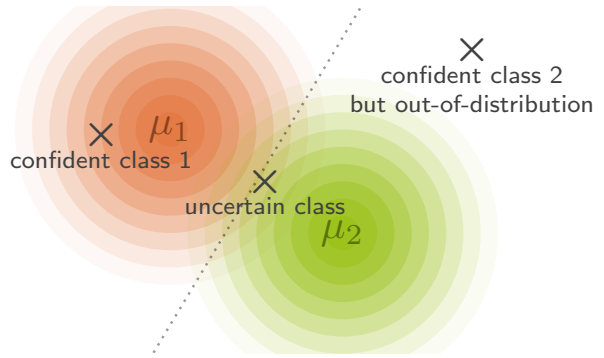


Figure 2: Illustration of the latent output space of a generative classifier. The two class likelihoods for $Y = \{1, 2\}$ are parameterized by their means $\mu_{\{1,2\}}$. The dotted line represents the decision boundary between the two classes. A confident, an uncertain, and an out-of-distribution sample is illustrated.

2 METHOD

In the following, upper case letters denote random variables (RVs) (e.g. U), lower case letters denote specific instances of that RV (e.g. u). The probability density function of an RV is written as $p(U)$, the evaluated density is written as $p(u)$ or $p(U = u)$ when ambiguous. All RVs are considered vector quantities.

2.1 Invertible NNs as Generative Classifiers

In this work we train an Invertible Neural Network (INN) g_θ , with some network parameters θ , since it is one of the few deep learning models that has a tractable Jacobian determinant, allowing for exact likelihood estimation. The INN can be any architecture such as GLOW (Kingma & Dhariwal, 2018), RealNVP (Dinh et al., 2017), NICE (Dinh et al., 2015), i-Resnet (Behrmann et al., 2019), etc., as long as the requirements, i.e. computationally efficient invertibility and a tractable Jacobian determinant, are fulfilled. Given the input X , an INN models a likelihood $q_\theta(X)$ by reparameterization in a latent space with prescribed latent distribution $p(Z)$. For normalizing flows, a common choice is $p(Z) = \mathcal{N}(0, 1)$. Given some input x , the change-of-variables formula gives

$$q_\theta(x) = q(Z = g_\theta(x)) \left| \det \left(\frac{\partial g_\theta}{\partial x} \Big|_x \right) \right|. \quad (1)$$

The Jacobian matrix will in the following be abbreviated as $\partial g_\theta / \partial x := J_\theta(x)$. We make this likelihood conditional, by making the latent distribution itself conditional on a discrete variable Y (in our case the class label). Thus, forming a Gaussian mixture model (GMM) $p(Z)$, where each mixture component is given by $q(Z|Y) = \mathcal{N}(\mu_Y, 1)$. The conditional likelihood is

Table 1: Comparing different models: Discriminative classifiers (DCs), Generative classifiers (GCs), Variational Information Bottleneck (VIB), and our Information Bottleneck Invertibel Neural Network (IB-INN).

	Standard DCs	Standard GCs	VIB	IB-INN (ours)
I. Classification Performance	✓	✗	✓	✓
II. Intrinsically well calibrated (i.e. good Uncertainties)	✗	(✓)	✗	✓
III. Out-of-Distribution (OoD) detection	✗	✓	✗	✓
IV. Generative Model	✗	✓	✗	✓
V. Controllable trade-off between I and II,III,IV above	✗	(✓)	✓	✓

now given by

$$q_{\theta}(x|y) = q(Z = g_{\theta}(x)|y) |\det(J_{\theta}(x))| \quad (2)$$

and we can access the marginal likelihood through $q_{\theta}(x) = \sum_y q_{\theta}(x|y) p(y)$.

Once a conditional likelihood model has been learned by an INN with GMM latent space, or any other class-conditional likelihood model, classification is straight forward to perform using Bayes' theorem:

$$q(y|x) = \frac{q_{\theta}(x|y) p(y)}{\sum_{y'} q_{\theta}(x|y') p(y')} . \quad (3)$$

This type of model, which estimates the class-conditional data likelihood to perform classification, is called a generative classifier (GC).

2.2 Information Bottleneck Loss

The Information Bottleneck (IB) objective \mathcal{L}_{IB} (Tishby et al., 2000), is defined in terms of the mutual information (MI) $I(V, W)$. In short, the MI quantifies the amount of information shared between two random variables. The IB is then

$$\mathcal{L}_{\text{IB}} = I(X, Z) - \beta I(Y, Z) . \quad (4)$$

In the general case, Z simply represents the internal data representation of some classification model. So, the objective attempts to maximize the MI between the desired classification output Y and representation Z in order to be able to perform the classification task. At the same time, it minimizes the MI between model input X and Z , essentially to ensure good generalization. In our case, naturally, Z will be the latent vector. The parameter β is a Lagrange multiplier, and controls the trade-off between the two objectives.

Application of IB to INNs: At this point, it is important to clearly distinguish the following distributions: in short, we will denote the true physical distributions as p , and the distributions modeled by the generative model as q . We define the *generator-MI* denoted I_{θ} , and equivalently the *generator-entropy* h_{θ} , in line with previous work (e.g. Belghazi et al., 2018). Hereby, the sampling distributions for the expectations

are p , and the densities are q :

$$h_{\theta}(V) = -\mathbb{E}_{v \sim p(V)} \log q(v) \quad (5)$$

$$I_{\theta}(V, W) = \mathbb{E}_{v, w \sim p(V, W)} \log \left(\frac{q(v, w)}{q(v)q(w)} \right) . \quad (6)$$

While Belghazi et al. (2018) use an alternative representation of the MI, the proof concerning strong consistency still applies, meaning $I_{\theta}(V, W)$ converges to $I(V, W)$ (the MI of the true data) after training, see Appendix.

In our case specifically, $p(X)$ denotes the physical distribution of input data, which is fundamentally unknown, and $p(Z)$ denotes its push-forward to Z -space by the INN g_{θ} . Conversely, $q(Z)$ describes the generative model's latent distribution (the GMM in our case), and $q(X)$ denotes its pull-back through g_{θ}^{-1} , i.e. the generated distribution, both of which are tractable.

Consider $I(X, Z)$: Note that the mutual information between X and Z is generally ill-defined for $Z = g_{\theta}(X)$ in the case of neural networks (see Amjad & Geiger, 2018), and especially for INNs. Specifically, $q(X, Z)$ is not a valid Radon-Nikodym probability density in this case. We resolve the degeneracy by introducing an additional noise term $\mathcal{E} = \sigma U$, with a scalar constant σ and standard normal distributed $U \sim \mathcal{N}(0, 1)$, which is added to the inputs X . This is motivated by practical experience: For normalizing flows and similar models, such noise is commonly added to the inputs, foremost because the quantization of the data otherwise leads to artifacts. In these cases, the noise is usually absorbed implicitly into X , while we write it explicitly, in line with e.g. Ho et al. (2019).

Adding the noise to the input of the transformation, we define $Z_{\mathcal{E}} = g_{\theta}(X + \mathcal{E})$, and now want to compute $I(X, Z_{\mathcal{E}})$. That is to say, how much can we say about the noise-free input X from the noisy latent vector $Z_{\mathcal{E}}$? Intuitively, this will depend on how the transformation treats the noise, relative to the noise-free signal: The more the noise is amplified, the more information content it takes up in $Z_{\mathcal{E}}$. As a result, the generator-MI with the noise-free inputs decreases. Indeed, this is precisely what we find. For small σ , we can series expand $Z_{\mathcal{E}}$, and can rearrange the objective to demonstrate its

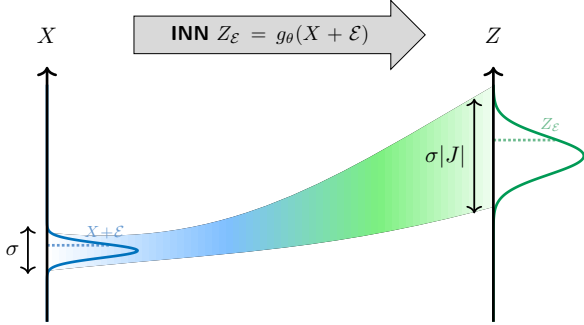


Figure 3: The more the noise is amplified in relation to the noise-free input, the lower the MI between noisy latent vector $Z_\mathcal{E}$ and noise-free input X .

behaviour:

$$I_\theta(X, Z_\mathcal{E}) = h_\theta(Z) - h(J_\theta \mathcal{E} | Z) + o(\sigma). \quad (7)$$

Note, $J_\theta \mathcal{E}$ denotes the matrix-vector product of the Jacobian and the noise \mathcal{E} . (Detailed derivation: see appendix.) This behaviour is just as we expected: To reduce the generator-MI, the network has to increase the $h(J_\theta \mathcal{E} | Z)$ term (i.e. amplify only the noise), without increasing the $h_\theta(Z)$ term by as much. The $h_\theta(Z)$ term can be kept low by learning the correct characteristics and properties of the input, so they do not have to be encoded in Z . This encourages it to be a generative model. It is simple to show that if this objective is minimized, the generator distribution matches the true physical distribution, $q_\theta(X) = p(X)$, and simultaneously $I_\theta(X, Z_\mathcal{E}) = I(X, Z_\mathcal{E})$.

From these considerations, we derive the following loss function. Note that due to our derivation with $\sigma \rightarrow 0$, we only need one network to be able to model all three densities in Eq. 6, and to not have to train a separate model for each.

$$\mathcal{L}_X(X) = h_\theta(Z_\mathcal{E}) - \mathbb{E}_{x \sim p(X+\mathcal{E})} \left[\log |\det J_\theta(x)| \right] \quad (8)$$

In the appendix, we show that optimizing this loss is equivalent to optimizing $I_\theta(X, Z_\mathcal{E})$ in the limit $\sigma \rightarrow 0$. Specifically, the dependence on σ can be separated out, independent of the network parameters, to arrive at the form in Eq. 8. As the actual value of σ no longer occurs in the loss, the noise can be made vanishingly small, to ensure that the limit case is satisfied to any desired precision. In practice, we simply imagine that it is smaller than the floating point accuracy, and do not have to add it explicitly. Note, we still de-quantize the data, but this is included in $p(X)$.

Consider $\mathbf{I}(\mathbf{Y}, \mathbf{Z})$: As we use the noisy inputs discussed above, we again replace Z with $Z_\mathcal{E}$. The computation is then straight forward,

$$I_\theta(Y, Z_\mathcal{E}) = h_\theta(Z_\mathcal{E}) - h_\theta(Z_\mathcal{E} | Y). \quad (9)$$

We explicitly write both entropies, and finally simplify the equation to form the second loss term

$$\begin{aligned} \mathcal{L}_Y(X, Y) &= \mathbb{E} \left[\log \left(\frac{q(z|y)}{\sum_{y'} q(z|y') p(y')} \right) \right] \quad (10) \\ &= \mathbb{E} \left[\log \left(\frac{q(z|y) p(y)}{\sum_{y'} q(z|y') p(y')} \right) - \log(p(y)) \right], \quad (11) \end{aligned}$$

where the expectation is taken over pairs $z, y \sim p(Z_\mathcal{E}, Y) = p(g_\theta(X + \mathcal{E}), Y)$. Note, that $q(z|y)$ are simply the components of the GMM, and can thus be easily evaluated. The reason for rearranging to Eq. 11 is due to the implementation explained in Appendix Sec. 7.3, and simultaneously highlights the relationship to Eq. 3.

2.3 Advantages of the IB-Loss

In this section we will interpret and discuss the nature of the loss function, derived above:

$$\mathcal{L}_{\text{IB}}(X, Y) = \mathcal{L}_X(X) - \beta \mathcal{L}_Y(X, Y). \quad (12)$$

We also form an intuitive understanding of why it is more suitable than the class-conditional negative-log-likelihood (‘class-NLL’) traditionally used for generative classifiers of this type. The findings are represented graphically in Fig. 4.

\mathcal{L}_X -term Comparing this term to the (unconditional) negative-log-likelihood loss used for standard normalizing flows, we see that the losses are almost identical, with the difference that $q(Z)$ is a GMM rather than a simple unimodal Gaussian. We conclude that this loss term encourages the INN to become an accurate likelihood model under the marginalized latent distribution and completely ignores any class content. Previous work on normalizing flows (e.g. Tabak & Turner, 2013) has shown that by minimizing this loss, the INN will become a model for the true (unconditional) data distribution.

\mathcal{L}_Y -term Examining Eq. 11, we see that for any z , the cluster centers (μ_Y) of the other classes are repulsed, while z and the correct cluster center are drawn together. Note that the class-NLL loss only captures the second aspect, and therefore has a much weaker training signal. We can also view this in a different way: by substituting $p(x|y) |\det(J_\theta(x))|^{-1}$ for $p(z|y)$ (see Eq. 2), the first summand of Eq. 11 simplifies to $\log p(y|x)$, since the Jacobian cancels out. This means that the \mathcal{L}_Y loss directly maximizes the correct class probability, while ignoring the data likelihood. Again, this improves the training signal, as Fetaya et al. (2019) showed that the data likelihood dominates the class-NLL loss, so that the discriminative aspect is not properly learned.

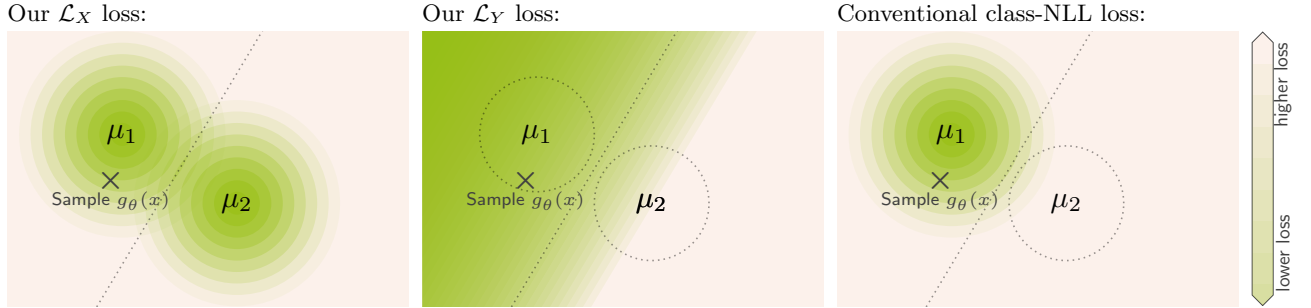


Figure 4: Illustration of the loss landscape according to our IB formulation (*left, middle*) and conventional class-conditional negative-log-likelihood (NLL) (*right*). The loss is shown for an input x belonging to class $Y = 1$, green areas correspond to low loss values.

Classical class-NLL loss The class-NLL loss encourages the INN to model each class separately. Fig. 4 illustrates how the loss does not have a visible class discriminatory nature. This is explained in more detail by Fetaya et al. (2019), who show that indeed the class-NLL loss causes a vanishingly small training signal for the class separation: points are only drawn towards the correct class, but there is no term separating them from the incorrect classes. For an unregularized model trained with class-NLL, this causes all cluster centers to collapse together, leading the INN to effectively just model the marginal data likelihood.

2.4 Practical Implementation

We learn μ_Y as a free parameter jointly with the remaining model parameters in an end-to-end fashion using the loss in Eq. 12. The entire training process is performed in log-space for numerical stability, as the likelihoods become both too large and too small otherwise (see Appendix Sec. 7.3 for details).

We apply two additional techniques while learning the model, label smoothing and loss rebalancing:

Label smoothing We observed that the individual class means μ_Y drift apart during training, because training with hard labels enforces the Gaussian mixture components to become perfectly separated. This can cause problems during training, as there is a high loss barrier between the clusters due to \mathcal{L}_X , preventing points from moving smoothly from one class to the other during training. To avoid this effect, we simply apply a small amount of label smoothing (Szegedy et al., 2016), where the one-hot training vectors are softened with $\alpha = 0.05$ in our case. This is enough to prevent the problem, and is our only form of regularization.

Loss rebalancing To avoid the laborious process of having to adjust hyperparameters for vastly different loss magnitudes, we employ the following rebalancing scheme: Firstly, we divide the loss \mathcal{L}_X by the number of dimensions of X . This ensures that \mathcal{L}_X remains in a similar range when changing e.g. the input image size,

as it scales linearly with the number of input dimensions. Secondly, we define a matching $\tilde{\beta} \equiv \beta / \dim(X)$. Lastly, we reweight the entire loss by a factor $2/(1+\tilde{\beta})$. This ensures that the loss keeps the same magnitude when changing $\tilde{\beta}$ over wide ranges. Thanks to this rebalancing scheme, we can use the same learning rate and hyperparameters for all experiments:

$$\mathcal{L}_{\text{IB}}(X, Y) = \frac{2}{1 + \tilde{\beta}} \left(\frac{\mathcal{L}_X(X)}{\dim(X)} + \tilde{\beta} \mathcal{L}_Y(X, Y) \right) \quad (13)$$

3 EXPERIMENTS

We construct our IB-INN by combining the design efforts of various previous works on INNs and normalizing flows. In brief, we use a Real-NVP design consisting of affine coupling blocks (Dinh et al., 2017), with added improvements from recent works, such as Kingma & Dhariwal (2018); Jacobsen et al. (2019, 2018); Ardizzone et al. (2019). A more detailed description of the architecture is provided in the appendix.

3.1 Comparison of Methods

In addition to the IB-INN, we train several alternative methods. For each, we use exactly the same INN model, or an equivalent feed-forward ResNet model. Every method has the exact same hyperparameters and training procedure, the only difference being the loss function, and the lack of invertibility for pure feed-forward models.

Feed-forward As a baseline, we train a feed-forward ResNet (He et al., 2016) with softmax cross entropy objective. Starting from the INN architecture, each affine coupling block is simply replaced by a ResNet block, using the exact same design for each residual subnetwork as for the INN’s subnetworks. Each invertible downsampling is replaced with a convolution with stride set to 2. We do this to ensure that the networks are as similar as possible, the only difference being the invertibility.

Variational Information Bottleneck (VIB) We

train the VIB, as presented by Alemi et al. (2017), using a feed-forward ResNet. Note that the authors define their β in the opposite way, by weighting $I_\theta(X, Z)$. For consistency we convert this to our definition of $\hat{\beta}$.

i-RevNet (Jacobsen et al., 2018) To rule out any differences stemming from the constraint of invertibility, we additionally train the INN as a standard softmax classifier, by projecting the outputs to class logits. This means, while it uses the INN architecture, it is not generative and trained just like a feed-forward classifier.

Class-NLL As a standard generative classifier, we firstly train an INN with a GMM in latent space completely naively as a conditional generative model, using the class-conditional maximum likelihood loss $\mathcal{L}_{\text{class-NLL}}(X, Y) = -\log(q_\theta(X|Y))$.

Secondly, we also train a regularized version, to increase the classification accuracy. The regularization consists of constraining the class centroids μ_Y to points on a sphere with a fixed radius. As the radius becomes comparable to the typical intra-class distances, the training signal for the classification is amplified. We therefore choose $\sqrt{\dim(Z)}$ as radius. See Fetaya et al. (2019) for details.

3.2 Quantitative measurements

In the following, we describe the quantitative scores reported in Table 2.

Calibration error In general, the calibration curve measures whether the confidence of a model agrees with its actual performance. It is computed by first binning all prediction outputs according to their predicted probability P , also called the *confidence*. Note that all outputs are included, not just the class with the highest predicted probability. For each bin, it is then recorded for which fraction of these samples the prediction was actually correct, Q . For a perfectly calibrated model, we have $P = Q$, e.g. predictions with 30% confidence are correct 30% of the time.

There are now various metrics to measure deviation from this perfect behaviour, and we largely adhere to those used by Guo et al. (2017). For instance, we can consider the expected calibration error $\text{ECE} = \sum_P N_P/N|P - Q|$ (N_P : count in bin P , N : total), and the maximum calibration error $\text{MCE} = \max_P |P - Q|$. However, there are some limitations to these metrics, as the ECE is dominated by the calibration in the low-confidence region $P \ll 1$, and the MCE is noisy due to the fact that only a single bin leads to the result.

To make the analysis more robust, we additionally introduce the *overconfidence* measure, which is characterized by a threshold, e.g. $P_{\text{conf}} \geq 0.995$ in our case, defining the region of potential overconfidence. We then measure the accuracy Q_{conf} of the predictions with higher confidence than the threshold, and define the overconfidence as $\text{OVC} = (1 - Q_{\text{conf}})/(1 -$

$P_{\text{conf}})$. For a correctly calibrated model, the error rate should be lower than indicated by the chosen confidence threshold, meaning there is an upper bound $\text{OVC} \leq 1$ that a correct model can possibly exhibit. If the model is overconfident, it has $\text{OVC} \gg 1$. Comparing all three metrics for different models, we find that the rankings of each metric are partly inconsistent, so we also include the geometric mean of all three (i.e. $\sqrt[3]{\text{ECE} \cdot \text{MCE} \cdot \max(1, \text{OVC})}$). The geometric mean is used because it properly accounts for the different magnitudes of the metrics. Note, that we only penalize the OVC if it is above the upper bound for a well-calibrated model.

Out-of-distribution (OoD) prediction entropy

For data that is OoD, we expect from a model that it returns uncertain class predictions, as it has not been trained on such data. In the ideal case, each class is assigned the same probability of $1/(\text{nr. classes})$. The performance measure commonly used for this, e.g. by Ovadia et al. (2019), is to measure this through the discrete entropy of the class prediction outputs $H(Y|X_{\text{OoD}})$, which should be as high as possible.

OoD detection score For OoD detection, we use the (unconditional) negative log-likelihood (NLL) predicted by each model as an outlier score. This is a basic approach, but also the most common in the generative classifier literature. For the VIB, the situation is different, as it cannot directly estimate $p(X)$ as opposed to a standard VAE, due to the missing reconstruction loss. As a substitute, we therefore only use the ELBO loss (also termed ‘info-loss’ in the VIB literature), that stems from the $I(X, Z)$ -term. Note, in the original VIB work, no OoD detection was performed, and the described approach is not standard practice. Hence we only list these results for completeness.

To summarize, for the OoD detection capabilities of each model we simply record the degree of separability between in-distribution data and OoD data. This means, for a random inlier and a random outlier, it is the probability that the outlier has a higher outlier score. This would be a detection score of 1.0 for perfectly separated in- and outliers, and 0.5 if each point is assigned a random score. Note that this definition is exactly equal to the widely used ROC-AUC metric.

OoD datasets The inlier dataset consist of CIFAR10 images, i.e. 32×32 colour images showing 10 object classes. Additionally we created four different OoD datasets, that cover different aspects, see Fig. 5. Firstly, we create a random 3D rotation matrix with an adjustable rotation angle α , and apply it to the RGB color vectors of each pixel of CIFAR10 images. We set a fixed value of $\alpha = 0.3\pi$ for quantitative comparisons. Secondly, we add random uniform noise with a small amplitude to CIFAR10 images, to see if minor alterations of the image statistics can also be detected as

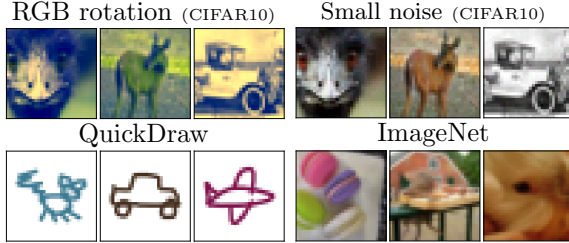


Figure 5: Examples from each of our four OoD datasets used in the evaluation. The inlier data are original CIFAR10 images.

OoD Thirdly, we use the QuickDraw dataset of hand drawn objects (Ha & Eck, 2018), and filter only the categories corresponding to CIFAR10 classes. We then color each grayscale line drawing randomly. This data represents a completely different image modality, but with the same semantic content. Lastly, we downscale the ImageNet validation set to 32×32 pixels. This constitutes a dataset of natural images with very similar image statistics to CIFAR10, but this time with completely different semantic content. However, we find that none of the models can reliably detect the ImageNet data as OoD, so we use this primarily to measure the prediction entropy behaviour on OoD data.

3.3 Effect of Beta

To study the trade-off between classification performance and modeling capabilities parameterized by $\tilde{\beta}$, we train 24 IB-INN models for different $\tilde{\beta}$ ranging from 0.02 to 50. For comparison, we also train corresponding VIB models, and summarize our findings in Fig. 8.

As expected, the classification accuracy improves as we increase $\tilde{\beta}$, while the uncertainty estimates become worse. The trend of OoD separability depends on the dataset: It is almost constant for the RGB rotated data, improves for the hand-drawn data, and degrades for the noisy data. This is due to whether the focus on class information is helpful in detecting OoD data, or whether simply modeling natural images suffices. The classification accuracy of the VIB stays almost constant over the whole range, and the uncertainties also show little variations, indicating that the used loss function is indeed only a rough bound on the true IB.

3.4 Quantitative Model Comparison

A comparison of all models is performed in Table 2 for CIFAR10 and CIFAR100. We point out that to our best knowledge, in the literature so far, generative classifiers have never been used for CIFAR100, as this is generally very challenging.

In summary, we find that the IB-INN has slightly worse classification performance than a standard DC, which



Figure 6: Each column shows a latent space interpolation between two images (leftmost and rightmost). Each row corresponds to a model trained with a different $\tilde{\beta}$. We find that the generative performance generally decreases with increased $\tilde{\beta}$.

is in line with the typical performance drop from feed-forward to invertible architecture (Gomez et al., 2017). However, the uncertainties in the form of calibration error and entropy on OoD data, are far superior. For ablation where only \mathcal{L}_Y is used ($\tilde{\beta} \rightarrow \infty$), the performance is more comparable to a standard DC, demonstrating that it is really the IB objective giving the improvements. In addition, the OoD detection is on par or better than for the other GCs. Furthermore, the GCs naively trained with class-NLL make no meaningful predictions, neither on CIFAR10 nor CIFAR100. While the regularized version achieves better accuracy, and maintains the OoD detection capabilities, the calibration and uncertainty is very poor. Lastly, we find that the VIB brings some improvement over a standard feed-forward model in terms of uncertainties, especially for CIFAR100, but still inferior to IB-INN.

3.5 Latent Space Exploration

To better understand what the IB-INN learns, we analyze the latent space in different ways. Firstly, Fig. 7 shows the layout of the latent space GMM through a linear projection. We find that the clusters of ambiguous classes, e.g. truck and car, are connected in latent space, to account for uncertainty. Secondly, Fig. 6 shows interpolations in latent space between two test set images, using models trained with different values of $\tilde{\beta}$. We observe that for low $\tilde{\beta}$, the IB-INN has a very well structured latent space, resulting in good generative capabilities and plausible interpolations. For larger $\tilde{\beta}$, the interpolation quality continually degrades.

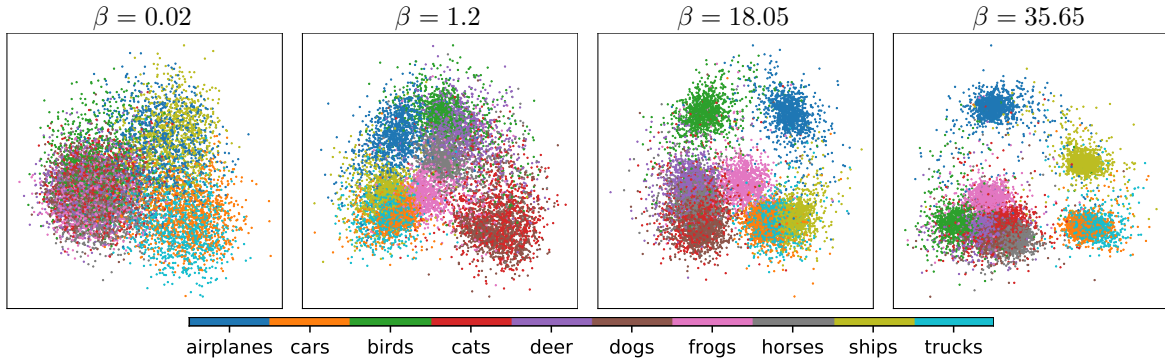


Figure 7: GMM Latent space behaviour by increasing $\tilde{\beta}$. The class separation increases with larger $\tilde{\beta}$. Note however, how ambiguous classes (truck and car) stay connected, to account for uncertainty.

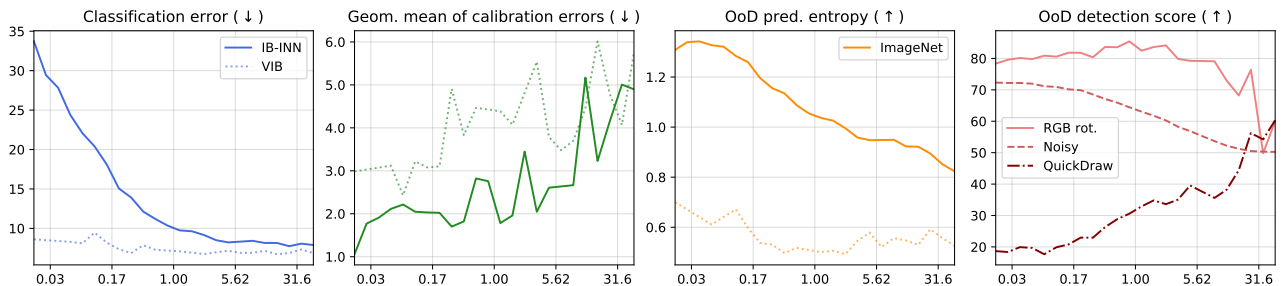


Figure 8: Effect of changing the parameter $\tilde{\beta}$ (x -axis) on the different performance measures (y -axis). The VIB results are added as dotted lines for comparison, except for OoD detection score. The inlier dataset is CIFAR10. The arrows indicate if a larger or smaller score is better. While the classification accuracy improves with $\tilde{\beta}$, the uncertainty measures grow worse. The trend for the OoD detection depends on the OoD data used, and whether the focus on class information is important for the detection. All curves shown separately in the appendix.

Table 2: Results on the CIFAR10 and CIFAR100 datasets. All models have the same number of parameters and were trained with the same hyperparameters. All values except entropy and overconfidence are given in percent. The arrows indicate whether a higher or lower value is better. The prediction entropy of the model trained with standard class-NLL is not taken into account, because the entropy is equally high on in-distribution data due to the poor classification performance. The OoD detection score for VIB is also not taken into account, see text.

CIFAR10	Classif. err. (\downarrow)	Calibration error (\downarrow)				OoD prediction entropy (\uparrow)					OoD detection score (\uparrow)				
		Geo. mean	Expec.	Max	Overc.	Geo. mean	RGB-rot	Draw	Noise	ImgNet	Geo. mean	RGB-rot	Draw	Noise	ImgNet
IB-INN (ours, $\tilde{\beta} = 1$)	9.88	1.969	0.93	8.20	0.00	0.865	0.86	1.07	0.59	1.02	54.03	86.5	21.3	86.3	53.6
IB-INN, only \mathcal{L}_Y ($\tilde{\beta} \rightarrow \infty$)	8.29	6.690	1.22	23.81	10.32	0.587	0.55	0.68	0.43	0.74	58.72	59.7	96.4	50.9	40.6
IB-INN, only \mathcal{L}_X ($\tilde{\beta} = 0$)	–	–	–	–	–	–	–	–	–	–	44.68	79.3	12.1	80.4	51.9
Class-NLL	84.98	62.016	11.21	86.16	247.00	(1.067)	(1.03)	1.22	0.97	1.06	48.55	80.2	18.6	71.6	52.0
Class-NLL (regularized)	20.57	24.176	3.93	20.30	177.33	0.002	0.00	0.00	0.00	0.00	48.95	82.0	16.1	79.1	54.9
VIB ($\tilde{\beta} = 1$)	7.29	4.466	0.68	27.83	4.71	0.342	0.35	0.38	0.19	0.52	(47.38)	(46.4)	52.2	50.0	41.7
Standard ResNet	6.76	5.656	0.73	40.61	6.12	0.344	0.35	0.44	0.18	0.51	–	–	–	–	–
i-RevNet	9.09	2.224	0.54	14.78	1.37	0.611	0.74	0.90	0.25	0.82	–	–	–	–	–

CIFAR100	Classif. err. (\downarrow)	Calibration error (\downarrow)				OoD prediction entropy (\uparrow)					OoD detection score (\uparrow)				
		Geo. mean	Expec.	Max	Overc.	Geo. mean	RGB-rot	Draw	Noise	ImgNet	Geo. mean	RGB-rot	Draw	Noise	ImgNet
IB-INN (ours, $\tilde{\beta} = 1$)	36.59	1.157	0.15	6.67	1.54	2.314	2.58	2.43	2.11	2.17	51.21	79.1	27.9	61.7	50.6
IB-INN, only \mathcal{L}_Y ($\tilde{\beta} \rightarrow \infty$)	33.86	1.171	0.15	4.68	2.34	2.394	2.53	2.62	2.17	2.29	60.92	68.6	99.3	49.5	40.8
IB-INN, only \mathcal{L}_X ($\tilde{\beta} = 0$)	–	–	–	–	–	–	–	–	–	–	39.67	74.2	8.5	77.9	50.3
Class-NLL	98.59	34.452	1.47	92.86	298.65	(1.982)	(1.89)	2.37	1.75	1.97	41.52	75.6	10.0	78.2	50.4
Class-NLL (regularized)	79.08	32.392	1.40	94.58	257.30	0.025	0.02	0.01	0.06	0.05	41.96	73.6	10.4	78.7	51.3
VIB ($\tilde{\beta} = 1$)	42.92	1.259	0.18	8.63	1.26	1.960	2.20	1.61	1.97	2.11	(48.00)	(43.0)	56.8	46.1	47.1
Standard ResNet	29.14	4.863	0.23	17.26	29.03	2.012	2.21	2.16	1.78	1.92	–	–	–	–	–
i-RevNet	34.27	2.880	0.24	17.76	5.50	1.762	2.16	1.71	1.55	1.69	–	–	–	–	–

4 RELATED WORK

Generative Classification: An in-depth analysis of the trade-offs between discriminative and generative models was first performed by Ng & Jordan (2001) and was later extended by Bouchard & Triggs (2004); Bishop & Lasserre (2007); Xue & Titterton (2010), who investigated the possibility of balancing the strengths of both methods via a hyperparameter. Promising applications of these ideas to natural language processing, based on neural networks, were recently presented by Shen et al. (2017); Yogatama et al. (2017); Wang & Wu (2018). Li et al. (2019) showed that generative classifiers may be more robust against adversarial attacks, and Hwang et al. (2019) demonstrated their robustness against missing data. On the other hand, Fetaya et al. (2019) found that conditional generative models based on normalizing flows have poor discriminative performance, making them unsuitable for solving classification tasks. In light of our work, we think that they are indeed able to achieve good classification accuracy.

Information Bottleneck: The IB was introduced by Tishby et al. (2000) as a tool for information-theoretic analysis and optimization of compression method. This idea was further expanded on by Chechik et al. (2005); Gilad-Bachrach et al. (2003); Shamir et al. (2010) and Friedman et al. (2013). A relationship between IB and deep learning was first proposed by Tishby & Zaslavsky (2015), and later experimentally examined by Shwartz-Ziv & Tishby (2017), who use IB to facilitate understanding of neural network behavior and training dynamics. A close relation of IB to dropout, disentanglement, and variational autoencoding was discovered by Achille & Soatto (2018), which led them to introduce Information Dropout as a method to take advantage of IB in discriminative models. The approximation of IB in a variational setting was proposed independently by Kolchinsky et al. (2017) and Alemi et al. (2017), who especially demonstrate improved robustness against adversarial attacks.

5 CONCLUSIONS

We addressed the application of the Information Bottleneck (IB) to Invertible Neural Networks (INNs) as a loss function. We find that we can formulate an asymptotically exact version of the IB, which results in an INN that is a generative classifier. From our experiments, we conclude that the IB-INN provides higher quality uncertainties and out-of-distribution detection, while reaching almost the same classification accuracy as conventional feed-forward methods and generally outperforms other supervised generative classifiers on CIFAR10 and CIFAR100.

6 ACKNOWLEDGEMENTS

LA received funding by the Federal Ministry of Education and Research of Germany project ‘High Performance Deep Learning Framework’ (No 01IH17002). UK and CR received financial support from the European Research Council (ERC) under the European Unions Horizon 2020 research and innovation program (grant agreement No 647769). We thank the Center for Information Services and High Performance Computing (ZIH) at Dresden University of Technology for generous allocations of computation time. Furthermore we thank our colleagues, Jens Mller and Jakob Kruse for their help and support.

References

- Alessandro Achille and Stefano Soatto. Information dropout: Learning optimal representations through noisy computation. *IEEE Trans. Pattern Anal. Mach. Intell.*, 40(12):2897–2905, 2018. doi: 10.1109/TPAMI.2017.2784440. URL <https://doi.org/10.1109/TPAMI.2017.2784440>.
- Alexander A. Alemi, Ian Fischer, Joshua V. Dillon, and Kevin Murphy. Deep variational information bottleneck. In *5th International Conference on Learning Representations, ICLR 2017, Toulon, France, April 24-26, 2017, Conference Track Proceedings*, 2017. URL <https://openreview.net/forum?id=HyxQzBceg>.
- Rana Ali Amjad and Bernhard C Geiger. How (not) to train your neural network using the information bottleneck principle. *arXiv preprint arXiv:1802.09766*, 2018.
- Lynton Ardizzone, Carsten Lüth, Jakob Kruse, Carsten Rother, and Ullrich Köthe. Guided image generation with conditional invertible neural networks. *CoRR*, abs/1907.02392, 2019. URL <http://arxiv.org/abs/1907.02392>.
- Jens Behrmann, Will Grathwohl, Ricky T. Q. Chen, David Duvenaud, and Jörn-Henrik Jacobsen. Invertible residual networks. In *Proceedings of the 36th International Conference on Machine Learning, ICML 2019, 9-15 June 2019, Long Beach, California, USA*, pp. 573–582, 2019. URL <http://proceedings.mlr.press/v97/behrmann19a.html>.
- Ishmael Belghazi, Sai Rajeswar, Aristide Baratin, R. Devon Hjelm, and Aaron C. Courville. MINE: mutual information neural estimation. *CoRR*, abs/1801.04062, 2018. URL <http://arxiv.org/abs/1801.04062>.
- Christopher Bishop and Julia Lasserre. Generative or discriminative? getting the best of both worlds. *Bayesian Statistics*, 8, January 2007. URL <https://www.microsoft.com/en-us/research/publication/generative-discriminative-getting-best-worlds/>.
- Christopher M. Bishop. *Pattern recognition and machine learning, 5th Edition*. Information science and statistics. Springer, 2007. ISBN 9780387310732.
- Vladimir Igorevich Bogachev, Aleksandr Viktorovich Kolesnikov, and Kirill Vladimirovich Medvedev. Triangular transformations of measures. *Sbornik: Mathematics*, 196(3):309, 2005.
- Guillaume Bouchard and Bill Triggs. The tradeoff between generative and discriminative classifiers. In *16th IASC International Symposium on Computational Statistics (COMPSTAT'04)*, pp. 721–728, 2004.
- Gal Chechik, Amir Globerson, Naftali Tishby, and Yair Weiss. Information bottleneck for gaussian variables. *J. Mach. Learn. Res.*, 6:165–188, 2005. URL <http://jmlr.org/papers/v6/chechik05a.html>.
- Thomas M Cover and Joy A Thomas. *Elements of information theory*. John Wiley & Sons, 2012.
- Nicolaas Govert De Bruijn. *Asymptotic methods in analysis*, volume 4. Courier Corporation, 1981.
- Laurent Dinh, David Krueger, and Yoshua Bengio. NICE: non-linear independent components estimation. In *3rd International Conference on Learning Representations, ICLR 2015, San Diego, CA, USA, May 7-9, 2015, Workshop Track Proceedings*, 2015. URL <http://arxiv.org/abs/1410.8516>.
- Laurent Dinh, Jascha Sohl-Dickstein, and Samy Bengio. Density estimation using real NVP. In *5th International Conference on Learning Representations, ICLR 2017, Toulon, France, April 24-26, 2017, Conference Track Proceedings*, 2017. URL <https://openreview.net/forum?id=HkpbnH9lx>.
- Ethan Fetaya, Jörn-Henrik Jacobsen, and Richard S. Zemel. Conditional generative models are not robust. *CoRR*, abs/1906.01171, 2019. URL <http://arxiv.org/abs/1906.01171>.
- Nir Friedman, Ori Mosenzon, Noam Slonim, and Naftali Tishby. Multivariate information bottleneck. *CoRR*, abs/1301.2270, 2013. URL <http://arxiv.org/abs/1301.2270>.
- Ran Gilad-Bachrach, Amir Navot, and Naftali Tishby. An information theoretic tradeoff between complexity and accuracy. In *Computational Learning Theory and Kernel Machines, 16th Annual Conference on Computational Learning Theory and 7th Kernel Workshop, COLT/Kernel 2003, Washington, DC, USA, August 24-27, 2003, Proceedings*, pp. 595–609, 2003. doi: 10.1007/978-3-540-45167-9_43. URL https://doi.org/10.1007/978-3-540-45167-9_43.
- Aidan N. Gomez, Mengye Ren, Raquel Urtasun, and Roger B. Grosse. The reversible residual network: Backpropagation without storing activations. In *Advances in Neural Information Processing Systems 30: Annual Conference on Neural Information Processing Systems 2017, 4-9 December 2017, Long Beach, CA, USA*, pp. 2214–2224, 2017. URL <http://papers.nips.cc/paper/6816-the-reversible-residual-network-backpropagation-without-storing-activations>.
- Chuan Guo, Geoff Pleiss, Yu Sun, and Kilian Q. Weinberger. On calibration of modern neural networks. In *Proceedings of the 34th International Conference on Machine Learning, ICML 2017, Sydney, NSW, Australia, 6-11 August 2017*, pp. 1321–1330,

2017. URL <http://proceedings.mlr.press/v70/guo17a.html>.
- David Ha and Douglas Eck. A neural representation of sketch drawings. In *6th International Conference on Learning Representations, ICLR 2018, Vancouver, BC, Canada, April 30 - May 3, 2018, Conference Track Proceedings*, 2018. URL <https://openreview.net/forum?id=Hy6GHpkCW>.
- Kaiming He, Xiangyu Zhang, Shaoqing Ren, and Jian Sun. Deep residual learning for image recognition. In *2016 IEEE Conference on Computer Vision and Pattern Recognition, CVPR 2016, Las Vegas, NV, USA, June 27-30, 2016*, pp. 770–778, 2016. doi: 10.1109/CVPR.2016.90. URL <https://doi.org/10.1109/CVPR.2016.90>.
- Jonathan Ho, Xi Chen, Aravind Srinivas, Yan Duan, and Pieter Abbeel. Flow++: Improving flow-based generative models with variational dequantization and architecture design. In *Proceedings of the 36th International Conference on Machine Learning, ICML 2019, 9-15 June 2019, Long Beach, California, USA*, pp. 2722–2730, 2019. URL <http://proceedings.mlr.press/v97/ho19a.html>.
- Kurt Hornik, Maxwell Stinchcombe, and Halbert White. Multilayer feedforward networks are universal approximators. *Neural networks*, 2(5):359–366, 1989.
- Iiwon Hwang, Dahuin Jung, and Sungroh Yoon. Hexagan: Generative adversarial nets for real world classification. In *Proceedings of the 36th International Conference on Machine Learning, ICML 2019, 9-15 June 2019, Long Beach, California, USA*, pp. 2921–2930, 2019. URL <http://proceedings.mlr.press/v97/hwang19a.html>.
- Aapo Hyvärinen and Petteri Pajunen. Nonlinear independent component analysis: Existence and uniqueness results. *Neural Networks*, 12(3):429–439, 1999.
- Jörn-Henrik Jacobsen, Arnold W. M. Smeulders, and Edouard Oyallon. i-revnet: Deep invertible networks. In *6th International Conference on Learning Representations, ICLR 2018, Vancouver, BC, Canada, April 30 - May 3, 2018, Conference Track Proceedings*, 2018. URL <https://openreview.net/forum?id=HJsjskMbOZ>.
- Jörn-Henrik Jacobsen, Jens Behrmann, Richard S. Zemel, and Matthias Bethge. Excessive invariance causes adversarial vulnerability. In *7th International Conference on Learning Representations, ICLR 2019, New Orleans, LA, USA, May 6-9, 2019*, 2019. URL <https://openreview.net/forum?id=BkfbpsAcF7>.
- Diederik P. Kingma and Prafulla Dhariwal. Glow: Generative flow with invertible 1x1 convolutions. In *Advances in Neural Information Processing Systems 31: Annual Conference on Neural Information Processing Systems 2018, NeurIPS 2018, 3-8 December 2018, Montréal, Canada*, pp. 10236–10245, 2018. URL <http://papers.nips.cc/paper/8224-glow-generative-flow-with-invertible-1x1-convolutions>.
- Artemy Kolchinsky, Brendan D. Tracey, and David H. Wolpert. Nonlinear information bottleneck. *CoRR*, abs/1705.02436, 2017. URL <http://arxiv.org/abs/1705.02436>.
- Yingzhen Li, John Bradshaw, and Yash Sharma. Are generative classifiers more robust to adversarial attacks? In *Proceedings of the 36th International Conference on Machine Learning, ICML 2019, 9-15 June 2019, Long Beach, California, USA*, pp. 3804–3814, 2019. URL <http://proceedings.mlr.press/v97/li19a.html>.
- Eric T. Nalisnick, Akihiro Matsukawa, Yee Whye Teh, Dilan Görür, and Balaji Lakshminarayanan. Do deep generative models know what they don’t know? In *7th International Conference on Learning Representations, ICLR 2019, New Orleans, LA, USA, May 6-9, 2019*, 2019. URL <https://openreview.net/forum?id=H1xwNhCcYm>.
- Whitney K Newey and Daniel McFadden. Large sample estimation and hypothesis testing. *Handbook of econometrics*, 4:2111–2245, 1994.
- Andrew Y. Ng and Michael I. Jordan. On discriminative vs. generative classifiers: A comparison of logistic regression and naive bayes. In *Advances in Neural Information Processing Systems 14 [Neural Information Processing Systems: Natural and Synthetic, NIPS 2001, December 3-8, 2001, Vancouver, British Columbia, Canada]*, pp. 841–848, 2001. URL <http://papers.nips.cc/paper/2020-on-discriminative-vs-generative-classifiers-a-comparison-of-logistic-regression-and-naive-bayes>.
- Yaniv Ovadia, Emily Fertig, Jie Ren, Zachary Nado, David Sculley, Sebastian Nowozin, Joshua V. Dillon, Balaji Lakshminarayanan, and Jasper Snoek. Can you trust your model’s uncertainty? evaluating predictive uncertainty under dataset shift. *CoRR*, abs/1906.02530, 2019. URL <http://arxiv.org/abs/1906.02530>.
- Robert J Serfling. *Approximation theorems of mathematical statistics*, volume 162. John Wiley & Sons, 2009.
- Ohad Shamir, Sivan Sabato, and Naftali Tishby. Learning and generalization with the information bottleneck. *Theor. Comput. Sci.*, 411(29-30):2696–

- 2711, 2010. doi: 10.1016/j.tcs.2010.04.006. URL <https://doi.org/10.1016/j.tcs.2010.04.006>.
- Peng Shen, Xugang Lu, Sheng Li, and Hisashi Kawai. Conditional generative adversarial nets classifier for spoken language identification. In *Interspeech 2017, 18th Annual Conference of the International Speech Communication Association, Stockholm, Sweden, August 20-24, 2017*, pp. 2814–2818, 2017. URL http://www.isca-speech.org/archive/Interspeech_2017/abstracts/0553.html.
- Ravid Shwartz-Ziv and Naftali Tishby. Opening the black box of deep neural networks via information. *CoRR*, abs/1703.00810, 2017. URL <http://arxiv.org/abs/1703.00810>.
- Christian Szegedy, Vincent Vanhoucke, Sergey Ioffe, Jonathon Shlens, and Zbigniew Wojna. Rethinking the inception architecture for computer vision. In *2016 IEEE Conference on Computer Vision and Pattern Recognition, CVPR 2016, Las Vegas, NV, USA, June 27-30, 2016*, pp. 2818–2826, 2016. doi: 10.1109/CVPR.2016.308. URL <https://doi.org/10.1109/CVPR.2016.308>.
- Esteban G Tabak and Cristina V Turner. A family of nonparametric density estimation algorithms. *Communications on Pure and Applied Mathematics*, 66(2):145–164, 2013.
- Naftali Tishby and Noga Zaslavsky. Deep learning and the information bottleneck principle. In *2015 IEEE Information Theory Workshop, ITW 2015, Jerusalem, Israel, April 26 - May 1, 2015*, pp. 1–5, 2015. doi: 10.1109/ITW.2015.7133169. URL <https://doi.org/10.1109/ITW.2015.7133169>.
- Naftali Tishby, Fernando C. N. Pereira, and William Bialek. The information bottleneck method. *CoRR*, physics/0004057, 2000. URL <http://arxiv.org/abs/physics/0004057>.
- Zheng Wang and Qingbiao Wu. An integrated deep generative model for text classification and generation. *Mathematical Problems in Engineering*, 2018, 2018.
- Jing-Hao Xue and D. M. Titterton. On the generative-discriminative tradeoff approach: Interpretation, asymptotic efficiency and classification performance. *Computational Statistics & Data Analysis*, 54(2):438–451, 2010. doi: 10.1016/j.csda.2009.09.011. URL <https://doi.org/10.1016/j.csda.2009.09.011>.
- Dani Yogatama, Chris Dyer, Wang Ling, and Phil Blunsom. Generative and discriminative text classification with recurrent neural networks. *CoRR*, abs/1703.01898, 2017. URL <http://arxiv.org/abs/1703.01898>.

Exact Information Bottleneck with Invertible Neural Networks: Getting the Best of Discriminative and Generative Modeling

– Appendix –

7 PROOFS AND DERIVATIONS

7.1 Strong Consistency of $I_\theta(U, V)$

In our case, we only require $I_\theta(X, Z_\mathcal{E})$ and $I_\theta(Z_\mathcal{E}, Y)$, but we show the consistency for two unspecified random variables U, V , as it may be of general interest. However, note that our estimator will likely not be particularly useful outside of our specific use-case, and other methods should be preferred (e.g. Belghazi et al., 2018).

For the joint input space $\Omega = \mathcal{U} \times \mathcal{V}$, we assume that \mathcal{U} is a compact domain in \mathbb{R}^d , and \mathcal{V} is either also a compact domain in \mathbb{R}^l (Case 1), or discrete, i.e. a finite subset of \mathbb{N} (Case 2). In Case 1, we assume that $p(U, V)$ is absolutely continuous, and in Case 2, $p(U|v)$ is absolutely continuous for all values of $v \in \mathcal{V}$.

We assume INNs g_θ following the coupling block design discussed e.g. in Dinh et al. (2017), see Sec. 8 for details. Although, it can also be some other normalizing flow type network, such as an autoregressive flow. The network parameter space Θ is a compact domain of \mathbb{R}^n . From the architecture, it follows that $g_\theta(u)$ is uniformly bounded. We can also conclude that g_θ and J_θ are continuous in both the inputs and parameters. The densities are parametrized in the usual way, prescribing a smooth latent distribution q , from the exponential family, or sum of components from the exponential family.

In Case 1, $q_\theta(U), q_\theta(V), q_\theta(U, V)$, the densities are all modeled separately, by three flows $g_\theta^{(U)}(u), g_\theta^{(V)}(u), g_\theta^{(UV)}(u, v)$. Although in our formulation, we are later able to approximate the latter two through the first.

In Case 2, we only model $q_\theta(U|V)$, and assume that $q_\theta(V)$ is either known beforehand and set to $p(V)$ (e.g. label distribution), or the probabilities are parametrized directly. Then $q_\theta(U, V) = q_\theta(U|V)q_\theta(V)$ and $q_\theta(U) = \sum_{v \in \mathcal{V}} q_\theta(U, v)$.

We define the empirical estimate using n samples to be

$$\hat{I}_\theta^{(n)}(U, V) = \frac{1}{n} \sum_i \frac{\log q_\theta(u_i, v_i)}{\log (q_\theta(u_i)q_\theta(v_i))}$$

with $(u_i, v_i) \sim p(U, V), i \in \{1, \dots, n\}$ (14)

To show that this estimator is strongly consistent, we use the two Lemmas below.

Lemma 1. *For any $\eta > 0$ and $\delta > 0$, there is an $N \in \mathbb{N}$ so that*

$$\Pr\left(|I_\theta(U, V) - \hat{I}_\theta^{(n)}(U, V)| < \eta\right) > 1 - \delta \quad \forall n \geq N \quad (15)$$

Proof. We have already assumed that u, v are bounded, as well as J_θ and g_θ (all three flows in Case 1). If the latent distribution is from the exponential family, or a sum thereof, $\log q_\theta(u)$ will then also be bounded, due to the expression for the density:

$$\log q_\theta(u) = \log q(z = g_\theta(u)) - \log |\det J_\theta(u)|, \quad (16)$$

analogously for $q_\theta(v), q_\theta(u, v)$ for Cases 1 and 2. Due to these properties, the uniform law of large numbers applies (Newey & McFadden, 1994, Lemma 2.4) and guarantees existence of an N to satisfy the condition for any choice of θ . \square

Lemma 2. *For any $\eta > 0$ there is a choice of flow network g_{θ^*} so that*

$$|I(U, V) - I_{\theta^*}(U, V)| < \eta \quad (17)$$

Proof. Writing out the definitions explicitly, and rearranging, we find

$$\begin{aligned} I_{\theta^*}(U, V) &= I(U, V) + D_{\text{KL}}(p(U)p(V) \| q_{\theta^*}(U)q_{\theta^*}(V)) \\ &\quad - D_{\text{KL}}(p(U) \| q_{\theta^*}(U)) - D_{\text{KL}}(p(V) \| q_{\theta^*}(V)) \end{aligned} \quad (18)$$

Shortening the KL terms to D_1, D_2 and D_3 for convenience:

$$|I_{\theta^*}(U, V) - I(U, V)| = |D_1 - D_2 - D_3| \quad (19)$$

$$\leq D_1 + D_2 + D_3 \quad (20)$$

$$\leq 3 \max(D_1, D_2, D_3) \quad (21)$$

At this point, we can simply apply results from measure transport that guarantee that a mapping g_θ exists that can make $\max(D_1, D_2, D_3)$ arbitrarily small by matching p and q_θ . See e.g. Hyvärinen & Pajunen (1999), Theorem 1 for an accessible proof, or Bogachev et al. (2005), Corollary 4.2 for a more in-depth approach. Hornik et al. (1989) Theorem 2.4 is applied to the coupling block subnetworks. \square

Proposition 1. *The empirical estimator of the MI as defined above is strongly consistent, meaning for any $\epsilon > 0$ and $\delta > 0$, there is an $N \in \mathbb{N}$ and choice of flow network g_{θ^*} so that*

$$\Pr\left(|I(U, V) - \hat{I}_{\theta^*}^{(n)}(U, V)| < \epsilon\right) > 1 - \delta \quad \forall n \geq N \quad (22)$$

Proof. The proof follows directly by applying the triangle inequality and Lemmas 1 and 2, choosing each $\eta = \epsilon/2$:

$$\begin{aligned} |I(U, V) - \hat{I}_{\theta^*}^{(n)}(U, V)| &\leq |I(U, V) - I_{\theta^*}(U, V)| \\ &\quad + |I_{\theta^*}(U, V) - \hat{I}_{\theta^*}^{(n)}(U, V)| \\ &< \frac{\epsilon}{2} + \frac{\epsilon}{2} = \epsilon \end{aligned} \quad (23) \quad (24)$$

□

As a side note, we require more knowledge of U and V to show whether $I_{\theta}(U, V)$ is either \geq or \leq than $I(U, V)$. Depending on this, the objective must either be minimized or maximized in practice during training. This is a clear disadvantage over e.g. MINE for the general case. However, in our special case it is simple to show that $I_{\theta}(X, Z_{\mathcal{E}}) \geq I(X, Z_{\mathcal{E}})$ (see Corollary 2).

7.2 Loss Function \mathcal{L}_X

Again, we use an INN g_{θ} , where the network parameter space Θ is a compact domain of \mathbb{R}^n . From the architecture, it follows that both $g_{\theta}(u)$ and the Jacobian J_{θ} are uniformly bounded. As J_{θ} is bounded, this also implies that g_{θ} is Lipschitz-continuous. The X input space \mathcal{X} is a compact domain in \mathbb{R}^d .

We have the loss function as defined in the paper,

$$\mathcal{L}_X(X) = h_{\theta}(Z_{\mathcal{E}}) - \mathbb{E}_{x \sim p(X)} \left[\log |\det J_{\theta}(x)| \right] \quad (25)$$

as well as its empirical estimate using n samples

We want to show that the network optimization procedure that arises from the empirical loss, specifically meaning the gradients w.r.t. network parameters θ , are consistent with those of $I_{\theta}(X, Z_{\mathcal{E}})$.

As before, we split up the proof into two Lemmas.

Lemma 3. *For any $\eta > 0$ and $\delta > 0$ there is an $N \in \mathbb{N}$ so that*

$$\Pr\left(\hat{\mathcal{L}}_X^{(n)}(X) - \mathcal{L}_X(X) < \eta\right) > 1 - \delta \quad \forall n \geq N$$

Proof. Using the same arguments as for Lemma 1, we can easily see that \mathcal{L}_X will be bounded, and changes continuously with θ , so the uniform law of large numbers applies. For the GMM specifically, we can see the boundedness as follows:

$$-\log(q(z)) \leq \max_y [(z - \mu_y)^2/2] + \text{const.} \quad (26)$$

With bounded $z = g_{\theta}(x)$. □

Lemma 4. *For any $\eta > 0$ there is an $s > 0$, so that*

$$|\mathcal{L}_X(X) - I_{\theta}(X, Z_{\mathcal{E}})| < \eta \quad \forall \sigma < s \quad (27)$$

Proof. In the following proof, we make use of the $o(\cdot)$ notation. See e.g. De Bruijn (1981).

We write $f(\sigma) = o(g(\sigma))$ ($\sigma \rightarrow 0$) iff for any $\epsilon > 0$, there exists a δ so that

$$\|f(\sigma)\| < \epsilon g(\sigma) \quad \forall \sigma \leq \delta. \quad (28)$$

To begin with, we use the invariance of I_{θ} under the homeomorphic transform g_{θ} . This can be easily verified, see e.g. Cover & Thomas (2012) Ch. 8, by inserting the change-of-variables formula into the definition. This results in

$$I_{\theta}(X, Z_{\mathcal{E}}) = I_{\theta}(Z, Z_{\mathcal{E}}) = h_{\theta}(Z_{\mathcal{E}}) - h_{\theta}(Z_{\mathcal{E}}|Z) \quad (29)$$

Next, we series expand $Z_{\mathcal{E}}$ around $\sigma = 0$. Recall $\mathcal{E} = \sigma U$. We can use Taylor's theorem to write

$$Z_{\mathcal{E}} = Z + J_{\theta}(Z)\mathcal{E} + o(\sigma^2) \quad (30)$$

We have written the Jacobian dependent on Z , but note that it is still $\partial g_{\theta}/\partial X$, and we simply substituted the argument. We put this into the second entropy term in Eq. 29, and then perform a zero-order von Mises expansion of h_{θ} . In general, the identity is

$$h(W + \xi) = h(W) + o(\|\xi\|) \quad (\|\xi\| \rightarrow 0), \quad (31)$$

and we simply put $\xi = o(\sigma^2)$. Intuitively, this is what we would expect: the entropy of an RV with a small perturbation should be approximately the same without the perturbation. See e.g. Serfling (2009), Ch. 6 for details. Effectively, this allows us to write the residual outside the entropy:

$$h_{\theta}(Z_{\mathcal{E}}|Z) = h_{\theta}(Z + J_{\theta}(Z)\mathcal{E} + o(\sigma^2)|Z) \quad (32)$$

$$= h_{\theta}(Z + J_{\theta}(Z)\mathcal{E}|Z) + o(\sigma^2) \quad (33)$$

$$= h_{\theta}(J_{\theta}(Z)\mathcal{E}|Z) + o(\sigma^2) \quad (34)$$

At this point, note that $q_{\theta}(J_{\theta}(Z)\mathcal{E}|Z)$ is simply a multivariate normal distribution, due to the conditioning on Z . In this case, we can use the entropy of a multivariate normal distribution, and simplify to obtain the following:

$$h_{\theta}(J_{\theta}\mathcal{E}|Z) = \mathbb{E} \left[\frac{1}{2} \log (2\pi \det(\sigma^2 J_{\theta} J_{\theta}^T)) \right] \quad (35)$$

$$= \mathbb{E} \left[\frac{1}{2} \log (2\pi \sigma^{2d} \det(J_{\theta})^2) \right] \quad (36)$$

$$= \frac{\log(2\pi)}{2} + d \log(\sigma) + \mathbb{E} [\log |\det J_{\theta}|]. \quad (37)$$

Here, we exploited the fact that $J_\theta(Z)$ is an invertible matrix, and used $d = \dim(Z)$. The expectations are still over $p(Z_\mathcal{E})$. Finally, as in practice we only want to evaluate the model once, we use the differentiability of J_θ to replace

$$\mathbb{E}[\log |\det J_\theta(Z)|] = \mathbb{E}[\log |\det J_\theta(Z_\mathcal{E})|] + o(\sigma). \quad (38)$$

The residual can be written outside of the expectation as we know it is bounded from our assumptions about g_θ and J_θ (Dominated Convergence theorem).

Putting the terms together, we obtain

$$I_\theta(X, Z_\mathcal{E}) = h_\theta(Z_\mathcal{E}) - \frac{\log(2\pi)}{2} - d \log \sigma - \mathbb{E}[\log |\det J_\theta|] + o(\sigma) \quad (39)$$

$$= \mathcal{L}_X(X) - \frac{\log(2\pi)}{2} - d \log \sigma + o(\sigma) \quad (40)$$

Lastly, we can write the following. Note, to allow for the last step we must ensure that the $o(\sigma)$ term is uniformly convergent to 0 over Θ . We know this is the case as g_θ is Lipschitz continuous and the outputs are bounded (ArzelaAscoli theorem).

$$\frac{\partial}{\partial \theta} \left(I_\theta(X, Z_\mathcal{E}) - \mathcal{L}_X(X) \right) = \frac{\partial}{\partial \theta} \left(-\frac{\log(2\pi)}{2} - d \log \sigma + o(\sigma) \right) \quad (41)$$

$$= \frac{\partial}{\partial \theta} \left(o(\sigma) \right) = o(\sigma) \quad (42)$$

□

As a side note, this derivation can also be performed in the opposite way, by transforming $Z_\mathcal{E}$ back to X -space, although this is not as illustrative and interpretable as the way shown above.

Proposition 2. *For any $\epsilon > 0$ and $\delta > 0$ there is an $N \in \mathbb{N}$ and $s > 0$, so that*

$$\Pr \left(\left\| \frac{\partial}{\partial \theta} (\hat{\mathcal{L}}_X^{(n)}(X) - I_\theta(X, Z_\mathcal{E})) \right\| < \epsilon \right) > 1 - \delta \quad \forall n \geq N \quad \forall \sigma < s \quad (43)$$

Proof. Putting together Lemmas 3 and 4, the definition of $o(\sigma)$, and the triangle inequality, directly proves the statement. □

Corollary 2.1. *Eq. 7 used in the paper holds:*

$$I_\theta(X, Z_\mathcal{E}) = h_\theta(Z) - h(J_\theta \mathcal{E} | Z) + o(\sigma). \quad (44)$$

Proof. We combine Eqs. 29 and 34 to get

$$I_\theta(X, Z_\mathcal{E}) = h_\theta(Z_\mathcal{E}) - h(J_\theta \mathcal{E} | Z) + o(\sigma). \quad (45)$$

we then perform the same Von Mises expansion of the entropy as before, writing

$$h_\theta(Z_\mathcal{E}) = h_\theta(Z) + o(\sigma) \quad (46)$$

This directly gives the result. □

Corollary 2.2. *The generator-MI $I_\theta(X, Z_\mathcal{E})$ is greater or equal than the true MI $I(X, Z_\mathcal{E})$ for all θ (corresponding to the minimization during training):*

$$I_\theta(X, Z_\mathcal{E}) \geq I(X, Z_\mathcal{E}) \quad (47)$$

The equality holds iff $p(X) = q_\theta(X)$

Proof. Firstly, note that the definition of the generator-entropy $h_\theta(X)$ is equivalent to the cross entropy between $p(X)$ and $q_\theta(X)$. Therefore, we can apply the well-known inequality from information theory, that any cross entropy is \geq the entropy, and equal iff the two distributions are the same (see Cover & Thomas (2012), Ch. 6). Using the invariance to homeomorphic transforms, and then writing out the definitions, we get

$$I_\theta(X, Z_\mathcal{E}) - I(X, Z_\mathcal{E}) = I_\theta(X, X+\mathcal{E}) - I(X, X+\mathcal{E}) \quad (48)$$

$$= h_\theta(X) - h(X) \quad (49)$$

$$\geq 0 \quad (50)$$

With equality iff $p(X) = q_\theta(X)$. □

7.3 Loss Implementation in Practice

In the following, we provide the explicit loss implementations, as there are some considerations to make with regards to numerical tractability. Specifically, we make use of the operations `softmax`, `log_softmax`, `logsumexp` provided by most deep learning frameworks, as they avoid the most common pitfalls.

The class probabilities $p(y)$ are characterized through a vector Φ , with

$$q(y) = \text{softmax}_k^y(\Phi_k), \quad (51)$$

where the subscript of the softmax operator denotes the variable to be summed over in the denominator, while the superscript defines which index is used for the enumerator. The use of the softmax ensures that w_y stay positive and sum to one. During training, Φ can either be learned as a free parameter, or it can be determined beforehand from the training label distribution. Note when learning it, that only the gradients w.r.t. the \mathcal{L}_X loss should be taken, as the \mathcal{L}_Y loss is exploited by setting $p(y) = 1$ for some fixed y , and 0 for all others. We further define $w_y \equiv \log p(y)$

With $z = g_\theta(x)$ in the following, we also have

$$\bullet \log q(y) = w_y = \text{logsoftmax}(\Phi)_y \quad (52)$$

$$\bullet \log q(z|y) = -\frac{1}{2}\|z - \mu_y\|^2 + \text{const.} \quad (53)$$

$$\bullet \log q(z) = \text{logsumexp}_{y'} \left(-\frac{\|z - \mu_{y'}\|^2}{2} + w_{y'} \right) + \text{const} \quad (54)$$

With this, the loss functions are evaluated as

$$\mathcal{L}_X(x) = \text{logsumexp}_{y'} \left(\frac{\|z - \mu_{y'}\|^2}{2} - w_{y'} \right) - \log J_\theta(x) \quad (55)$$

$$\mathcal{L}_Y(x, y) = \text{logsoftmax}_{y'}^y \left(-\frac{\|z - \mu_{y'}\|^2}{2} + w_{y'} \right) - w_y \quad (56)$$

8 NETWORK ARCHITECTURE

As in previous works, our INN architecture consists of so-called *coupling blocks*. In our case, each block consists of one affine coupling (Dinh et al., 2017), illustrated in Fig. 9, followed by random and fixed soft permutation of channels (Ardizzone et al., 2019), and a fixed scaling by a constant, similar to ActNorm layers introduced by Kingma & Dhariwal (2018). For the coupling coefficients, each subnetwork predicts multiplicative and additive components jointly, as done by Kingma & Dhariwal (2018). Furthermore, we adopt the soft clamping of multiplication coefficients used by Dinh et al. (2017).

For downsampling blocks, we introduce a new scheme, whereby we apply the i-RevNet downsampling (Jacobsen et al., 2018) only to the inputs to the affine transformation (u_2 branch in Fig. 9), while the affine coefficients are predicted from a higher resolution u_1 by using a strided convolution in the corresponding subnetwork. After this, i-RevNet downsampling is applied to the other half of the channels u_1 to produce v_1 , before concatenation and the soft permutation. We adopt this scheme as it more closely resembles the standard ResNet downsampling blocks, and makes the downsampling operation at least partly learnable.

We then stack sets of these blocks, with downsampling blocks in between, in the manner of [8, down, 25, down, 25]. Note, we use fewer blocks for the first resolution level, as the data only has three channels, limiting the expressive power of the blocks at this level. Finally, we apply a discrete cosine transform to replace the global average pooling in ResNets, as introduced by Jacobsen et al. (2019), followed by two blocks with fully connected subnetworks.

We perform training with SGD, learning rate 0.1, momentum 0.9, and batch size 128, as in the original

ResNet publication by (He et al., 2016). We train for 450 epochs, decaying the learning rate by a factor of 10 after 150, 250, and 350 epochs.

9 ADDITIONAL EXPERIMENTS

In Figure 10 we show the trajectory of a sample in latent space, when gradually increasing the RGB-rotation OoD augmentation used in the paper. It travels from in-distribution to out-of-distribution.

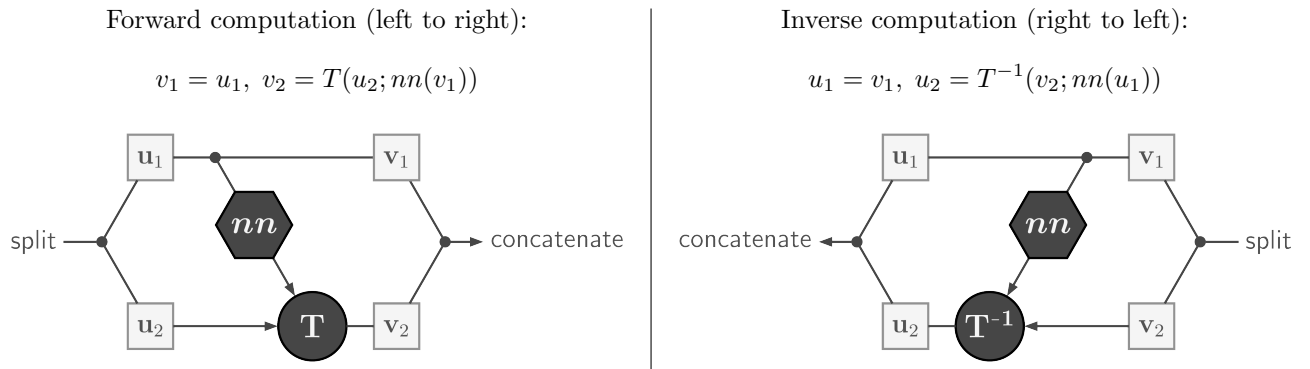


Figure 9: Illustration of a coupling block. T represents some invertible transformation, in our case an affine transformation. The transformation coefficients are predicted by a subnetwork (nn), which contains fully-connected or convolutional layers, nonlinear activations, batch normalization layers, etc., similar to the residual subnetwork in a ResNet (He et al., 2016). Note that the subnetwork does not have to be inverted itself.

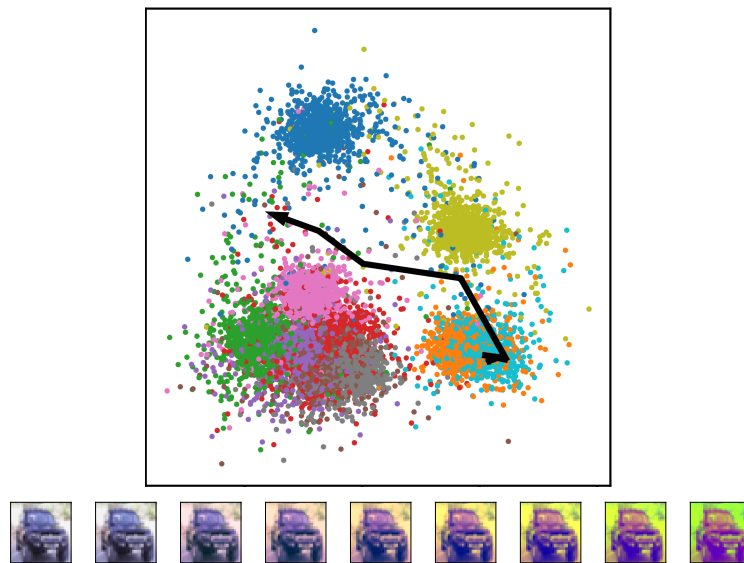


Figure 10: The scatter plot shows the location of test set data in latent space. A single sample is augmented by rotating the RGB color vector as described in the paper. The small images show the successive steps of augmentation, while the black arrow shows the position of each of these steps in latent space. We observe how the points in latent space travel further from the cluster center with increasing augmentation, causing them to be detected as OoD.